ORIGINAL ARTICLE – NANOMATERIALS

CrossMark

Soft, Self-Assembly Liquid Crystalline Nanocomposite for Superior Switching

Kaushik Pal[1] · Sami Sajjadifar[2] · Mohamed Abd Elkodous[3] · Yakubu Adekunle Alli[4] · Fernando Gomes[5] ·
Jaison Jeevanandam[6] · Sabu Thomas[7] · Alexander Sigov[8]

Abstract

Liquid crystal (LC) has long been a feature in Materials Science and Nanotechnology, have recently been extended into the appealing domain of complex hybrid materials. The crystalline structural effects of alkoxy chain lengths and the mesogen properties of hydrogen-bonded (n-OBASA) complexes ($n = 5,6,7$) have been investigated in recent studies. The LC-based hybrid nanocomposite materials–obtained by the homogeneous dispersion of zinc oxide nanowires (ZnO NWs) as a dopant into hydrogen-bonded liquid-crystalline compounds—seem to be particularly promising in this article. Optimizing the geometry of surface stabilizing electro-optic, LC cell reveals the typical intermolecular hydrogen bond (H-bond) formation. Here, we explore molecular-colloidal hybrid composite matrix formed from LCs and dilute dispersions of orientation-ordered ZnO NWs, for eventual potential application in smart switchable display devices. In addition, we investigated the structural, dielectric and optical properties of the nanocomposite, and electro-optical studies which were performed by exploiting the potential during the conditions before the opening of spectrum acquisition. Our novel findings confirm that the electric field induces a charge transfer of the LC molecules to the nanomaterial, which acts as a trap for ionic charges. This effect may be utilized to achieve superior switching operation that is electro-optically tunable. Such dynamic novel switching could be harnessed in smart LCD technology and pave the way towards innovative display modulation techniques.

✉ Kaushik Pal
  kaushikphysics@gmail.com;
  kaushikpaul.nano@bharathuniv.ac.in

1   Department of Nanotechnology, Bharath Institute of Higher
    Education and Research(BIHER), Bharath University, 173
    Agharam Road, Selaiyur, Chennai, Tamil Nadu 600073,
    India

2   Department of Chemistry, Payame Noor University (PNU),
    Ilam, P.O. Box 19395-4697, Tehran, Iran

3   Center for Nanotechnology (CNT), School of Engineering
    and Applied Sciences, Nile University, Sheikh Zayed, Giza,
    Egypt

4   Department of Chemistry, College of Physical Sciences,
   Federal University of Agriculture, Abeokuta, Ogun State,
    Nigeria

5   Instituto de Macromoléculas:Professora Eloisa Mano, Centro
    de Technologia-Cidade Universitária, Av. Horacio Macedo,
    2030, Bloco J.LaBioS Centro de Tecnologia, Rio de Jenerio,
    Brazil

6   Department of Chemical Engineering, Curtin University,
    CDT250, 98009 Miri, Sarawak, Malaysia

7   IIUCN, School of Chemical Sciences, Mahatma Gandhi
    University, Kottayam, Kerala 686560, India

8   Department of Nanoelectronics, MIREA - Russian
    Technological University, Prospekt Vernadskogo, 78,
    Moscow, Russian Federation 119454

Graphical abstract
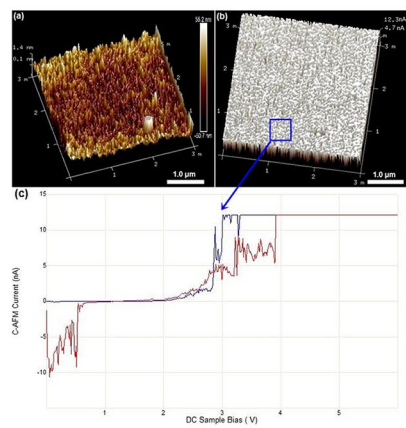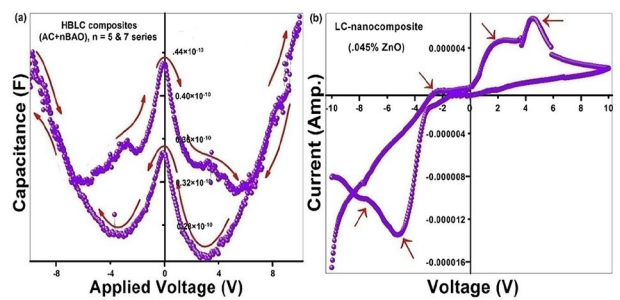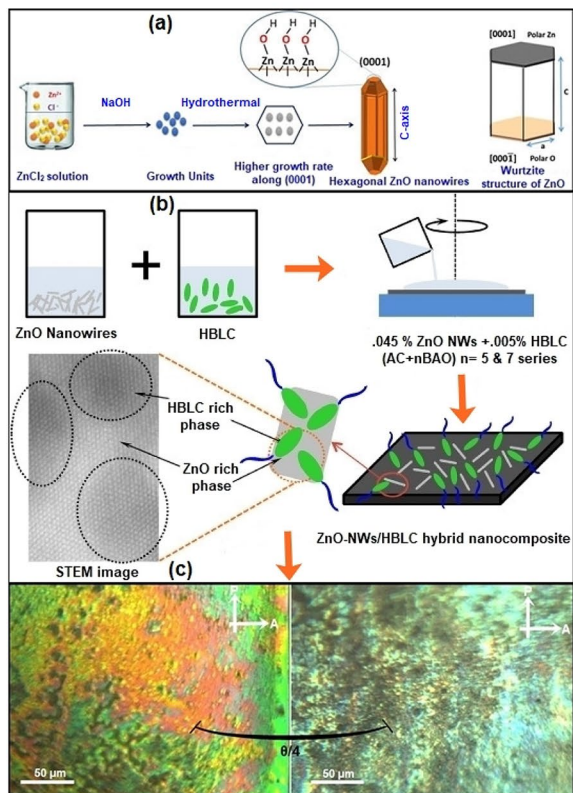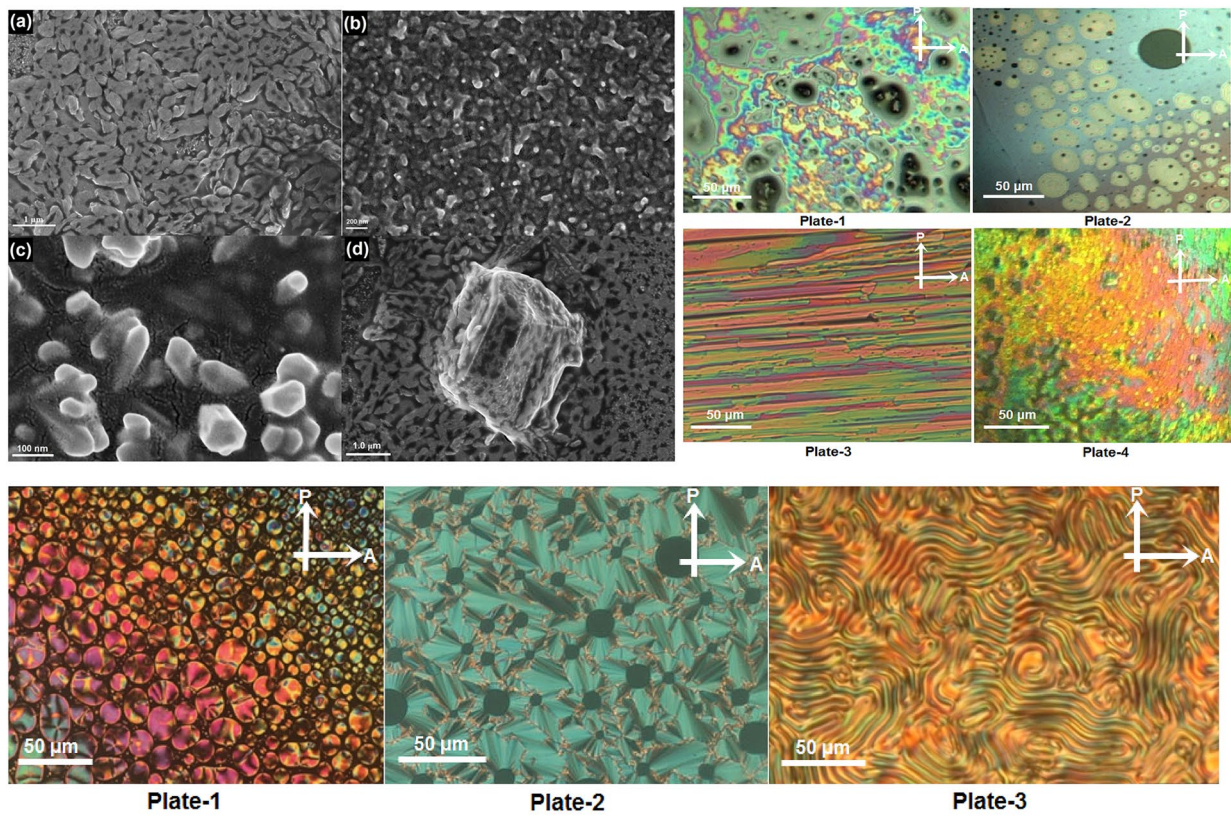
1 Introduction

Elements exist in nature in different states, including solid, liquid and gas. These states are distinguished by the degree and type of ordering of the constituent building blocks with respect to their neighbours.

Crystalline solids have highly ordered structures, while gases show no positional or orientation order at all. The liquid state exhibits short-range, but no long-range ordering happens due to a certain regularity in the arrangement of the neighbouring atom. In between the solid and liquid states is an intermediate mesophase that demonstrates long-range orientation order; sometimes these mesophases exhibit additional positional order. Liquid crystals (LCs), which consist of molecules with high configuration anisotropy, are the examples of such mesophases. Due to their strong symmetrical shape, LC molecules are generally considered as rigid rods or ellipsoids of revolution. Liquid crystalline materials can be broadly categorized into two types: thermotropic and lyotropic. Thermotropic liquid crystals are oily to the touch, and are also composed of organic molecules. They can exist either as single- or multi-component compounds and are particularly valuable in display technology, with approximately 90% of the world's display market made up of various forms of LC.

Soft, self-assembly functional LC materials exhibit both order and mobility at the molecular, supra-molecular and macroscopic levels [1–3]. Significant attention has been focused on the potential use of nanomaterial-dispersed LC hybrid composites for device modulation. As a result of this effort, ZnO NWs with their highly controllable morphology, have recently arisen as an exceptionally promising class of materials. The combination of ZnO NWs with increasingly effective techniques for homogeneously dispersing nanowires in liquid-crystalline materials has enabled the use of low-cost chemical synthesis routes in a wide assortment of potential applications, from the deposition of highly uniform layers and heterostructures to cutting-edge advances.

It has been known for past decades that the arrangement of LC molecules can be tuned using various techniques, for example, laser etching [4] electron-beam etching [5], micro rubbing [6], dip-pen lithography [7], rigiflex lithography [8], and delicate lithography [9].While such approaches enable a greater degree of control over the particle arrangement–for example, over the pre-tilt angle, anchoring energy and multi-stability—than conventional approaches, the performance of LC devices based on such a progression of surface-designed arrangement layers is inferior to that of LCDs containing polyimide (PI) arrangement layers [10]. Such devices are expected to benefit from the novel properties offered by soft self-assembling LCs and ZnO NWs.

Extensive efforts in Materials Science research such as improving our comprehension of nanomaterial fabrication, as well as the fundamental properties of LCs. One end goal is to exploit the energetic properties of NWs by incorporating them into LC mixtures in order to promote the formation of a typical complex hybrid structure. A suitable organic coating can provide robustness against aggregation as well as other critical features such as solubility, modularity, and optical and self-assembly properties.

ZnO nanowires which can be dispersed into LCs are made of submicron droplets of hydrogen-bonded liquid crystal (HBLC) compound that are implanted within a hybrid composite framework. In the absence of external fields, the LC atoms involved in nanomaterials dispersed liquid crystal (NDLC) hybrid composite for switchable device are arranged arbitrarily, the scattering of light dominates, and the material appears opaque. The application of stable electric field causes the LC atoms to align so that light transmission through the NDLC sample increases. The electro-optical behaviour and the simple handling and adaptability of NDLCs which are the reasons of nanocomposites have been considered for use in a wide range of potential applications in Nanoengineering and high-tech smart display device modulation, including smart windows, optical shutters, diffractive optics, photo-refractive systems, micro-displays, potential nuclear-radiation detectors, and flexible displays [11–15]. External disturbances influence the arrangement of LC atoms, which can impact the electro-optical properties of the displays. The utilization of noble-metal NWs as dopants in the LC microstructure is especially important because of the possibility of surface plasmon excitation [16–19] at the NW/LC interface and its impact on the electro-optical properties of the NDLCs.

One of the most recent researches has aimed to develop unique methodologies for shape- and size-uniform nanoscale self-assembly protocols. The progressive self-assembly of nanomaterial structures, as we described here, is a topic of great interest in the field of LCs. Due to their exceptional nature, LCs are suitable candidates for the matrix-guided synthesis and self-assembly of nanoscale materials, since the liquid crystalline state combines the desirable properties with versatility at the subatomic (nanoscale) level, facilitating some of the early trends emerge in this relatively smart technology field. This article presents a variety of materials that we used to grant a mesogenic nature of the hybrid composite materials. These materials were differ from their type of ligand coating.

2 Experimental Details

2.1 Materials design and Nanofabrication Strategy

All the basic chemical ingredients which were utilized as a part of this examination were of high virtue (99.5%) analytical grade, monetarily accessible and used as received without

further purification processing. High yield ZnO nanomaterials were synthesized and performed by the Professor K. Pal and his co-worker's research techniques [20–22]. Further fabrication of ZnO/HBLC dispersed-hybrid compounds were obtained by employing vigorous and uniform stirring by a magnetic stirrer and partially employed an ultrasound bath vibration for complete himogenious mixture in a cost-effective chemical assisted route.

2.2 Preparation of ZnO Nanowires Assembly of Liquid Crystalline Hybrid Composite

All the hybrid complexes are introduced in this manuscript have been combined with the guide of technique accessible during in past decades LC group [23]. Intermolecular hydrogen bonded LCs were blended utilizing two moles of p-n-alkoxy benzoic acids (nOBA), with one mole of suberic corrosive in N,N-dimethyl formamide (DMF) individually. Next, they have been subjected to steady mixing for 12 h at a surrounding temperature at 30°C till a dense white precipitation obtained. The white crystalline crude complexes have been collected by expelling by-product DMF and recrystallized using dimethyl sulfoxide (DMSO) and the yield fluctuated from 80 to 85%. The FT-IR range was recorded in the recurrence region 400–4000 cm^{-1} by utilizing KBr pellets (ABB FTIR MB 3000) and dissected by the MB 3000 85 programming. The development of multimer is investigated by recrystallization of the desired item. This core experiment manages nanomaterials including homologous arrangement of hydrogen reinforced liquid crystal (HBLC) formed between azelaic acid and p-n-heptyloxy benzoic acids also referred to as 'AC+nBAO', where carbon numbers, n=5 and 7, and m=7 for 'AC', the original chemical formula as stated follows:
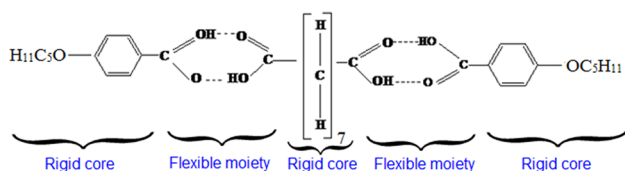
The chemical reactions are stated below:
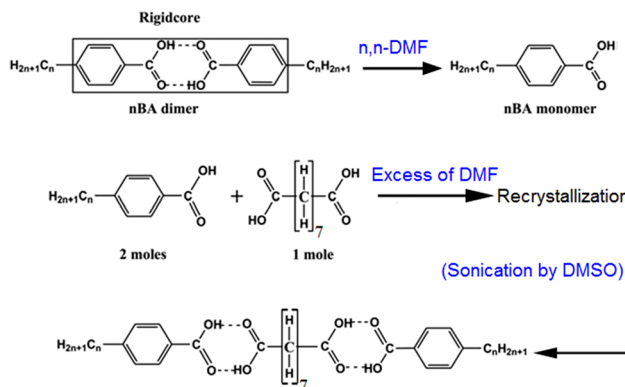
Thus, we are investigating the fundamental ideas that support this current trend of technological progress with a typical overview towards nanocomposite materials synthetic routes. While achieving sophisticated controllable growth dynamics, molecular orientations and uniform arrangement of LC atoms with a normal pre-tilt angle on a polyimide (PI) layer is a vital advance in production of LCD's [24, 25]. The capacity of LCD depends on the correct treatment of the limiting surface for precise orientation of the LC molecules. Mechanical rubbing has been generally used to furnish topographical micro-grooves that empower the uniaxial homogeneous or homeotropic alignment of LC [26] aspects as a novel approach for the ordering of LC atoms.

2.3 Simulated Patterns of Liquid Crystal

Two-dimensional simulations of the coarsening process of the isotropic/smectic-A phase transition are presented using a high-order Ginzburg–Landau model [27–32] for the phase transition dynamics in liquid crystalline optical materials. This model is able to emulate phase transitions among isotropic, nematic, smectic A and smectic C phases with controlling few parameters. Based on this model, we may exhibit numerical simulations as following Fig. 1a–c. Two-dimensional simulations of the coarsening process of the isotropic/smectic-A phase transition are presented using a high-order Landau-de Gennes type free energy model. The defect annihilation laws for smectic disclinations in Fig. 1a, elementary dislocations Fig. 1b, and total dislocation content are determined. The computed evolution of the orientational correlation length and disclination density which can be found in Fig. 1c are to be in agreement with the previous experimental observations illustrating that disclination interactions dominate the coarsening process.

Hence, the mechanism of smectic disclination movement, limited by the absorption and emission of elementary dislocations, is found to be facilitated by curvature walls connecting interacting disclinations. At intermediate times in the coarsening process, split-core dislocation formation and interactions displaying an effective disclination quadrupole configuration are observed. This work provides the framework for further understanding of the formation and dynamics of the diverse set of curvature defects observed in smectic liquid crystals and other layered material systems. Schematics of the different layer structures (highly magnified image of Fig. 1a) in the vicinity of the elementary dislocation were individually visible as depicted in Fig. 1d.
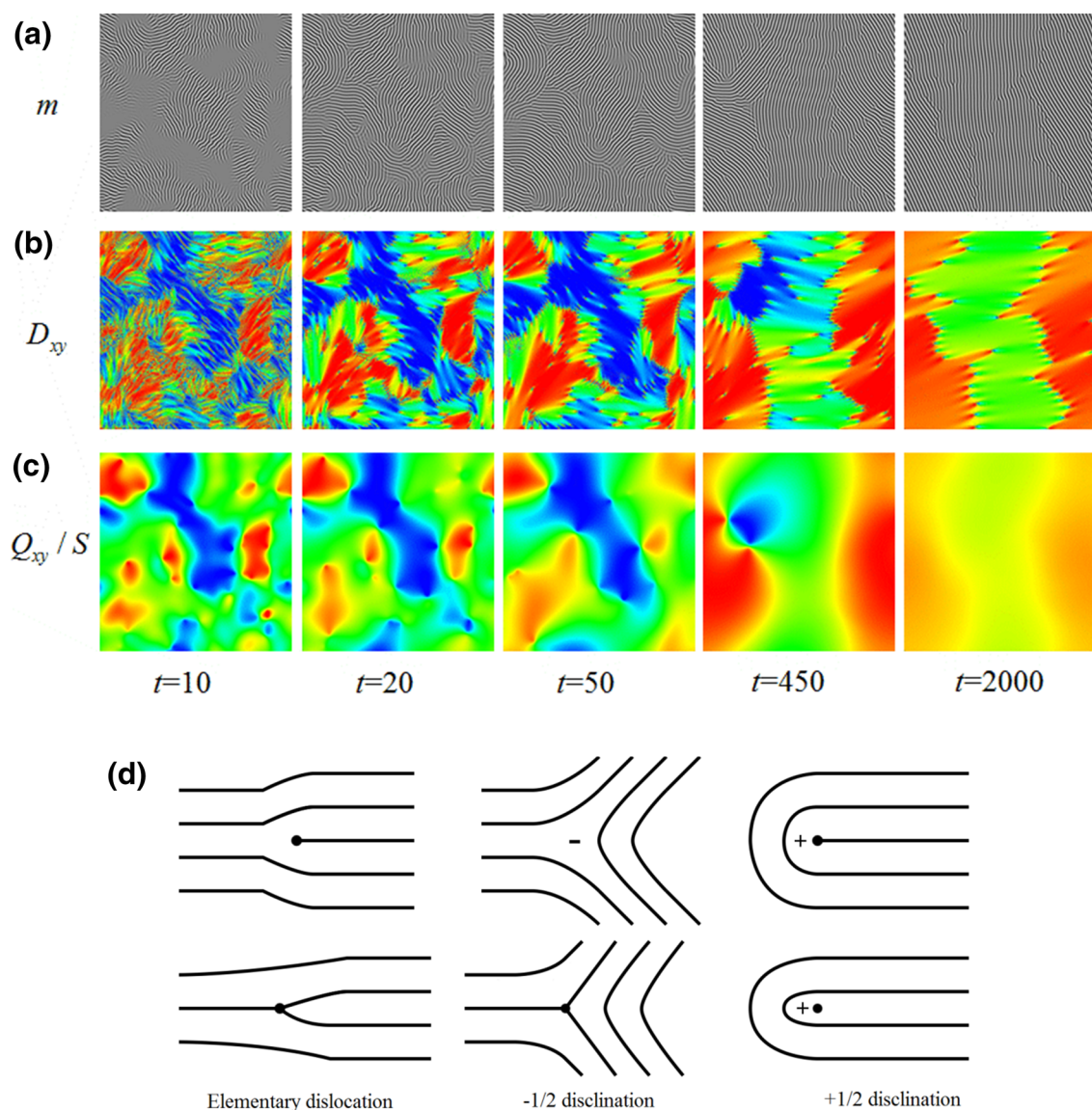
Fig. 1 Simulated patterns of the molecular orientation of different states of matter (solid, liquid and isotropic) **a** smectic order parameters, **b** dislocations, and **c** disclinations [27], **d** different layer structures in the vicinity of the elementary dislocation cores of strength

2.4 Photo-Refractive ITO-LC Electro-Optic Cells for Switchable Device Modulation

The planar aligned electro-optic device was then created by utilizing ZnO nanowires assembly homogeneous dispersion with HBLCs (AC + nBAO; n = 5 and 7) series of hybrid nanocomposite on conducting ITO glass films as one of the transparent electrodes. This is actually tunable electro-optical properties of U-shaped-alignment (USA) in-plane switching (IPS) of nanomaterials dispersed liquid crystal (NDLC) devices are successfully developed by adjusting the curing voltage and the surface-anchored cross linking monomer concentration during the polymerization process. The substrate is a glass slide covered by using an ITO. Both of the substrates are covered with a polymer arrangement layer that is consequently prepared and after that unidirectional rubbed (ITO-covered substrate just), the end goal advanced uniform sequence of the thin-film executive. The surface stabilized switchable device of photo-refractive ITO LC cells is then capillary-filled with ZnO nanowires/HBLC nanocomposite materials. Utilizing a typical inclination voltage over the thin-film layer distorts the crystal alignment, changing the adequate birefringence of the device and modifying the transmitted light intensity. The approximate thickness is 2.5 μm for the fabricated LC cell.
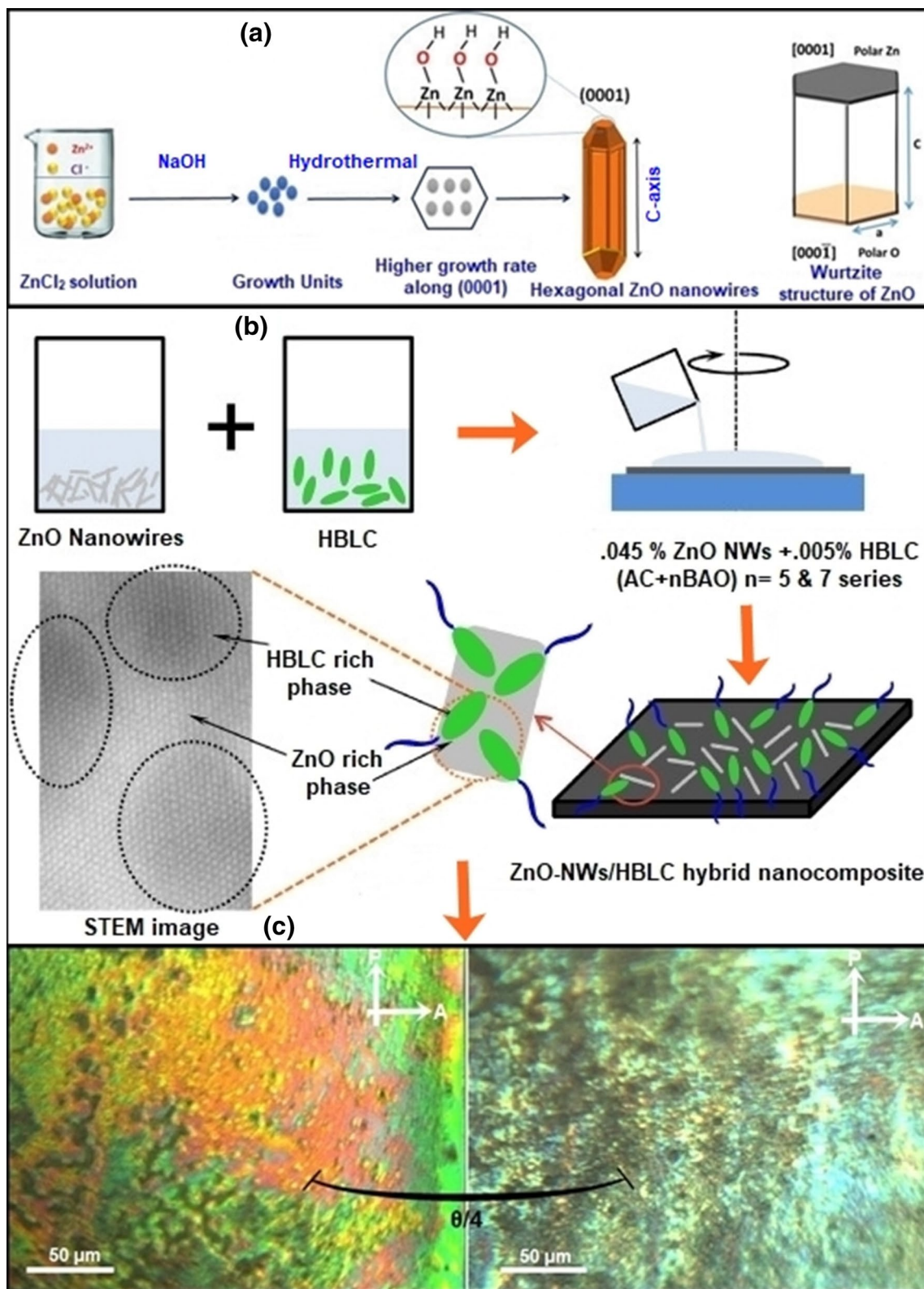
A controlled example, with an opening in the metallization and not capped by liquid crystal dopant ZnO nanowires self-assembly chemical interaction was schematically depicted in Fig. 2a. Hence, it is revealed that host ZnO rich phase nanowires contained with nm-sized LC-rich phases are identified in a scanning transmission electron

◄**Fig. 2** **a** Schematic of the growth dynamics of ZnO NWs was prepared via a hydrothermal approach coupled with a chemically-assisted technique, **b** ZnO/LC hybrid nanocomposite. The smooth dispersion of the homogeneous solution shown in the STEM image indicates the rich mesomorphism of the hybrid nanocomposite with ZnO NWs dispersed in HBLC, **c** Polarizing optical microscopy images showing nanosheets with marbled textures obtained at a temperature of 112.5°C. The surface sustained an in-plane switching response of ITO electro-optical cells induced by an external bias of 0–5 V. Optical switching between the 'ON' (≥ 5 V) and 'OFF' (≤ 0 V) states appeared under a cross polarizer in a switchable device

microscope (STEM) images detected on the ITO surface, and liquid crystalline materials generally have several common characteristics. Among these are rod-like molecular structure, rigidness of the long axis, and strong dipoles and easily polarizable substituent. So, LC molecules were homogeneously dispersed by ZnO nanowires whose chemical protocols were explored in the Fig. 2b. Hence, polarizing optical microscopy (POM) which explored the ZnO/HBLC doped-nanocomposite on the surface moderation treatment investigation, which was responsible for the photo refractive ITO-LC cell of effective exchanging ('ON' and 'OFF' state), was utilized by externally applied bias field under cross polarizer. At room temperature, the ZnO/HBLC-hybrid composite matrix which is frozen due to strong confinement of ZnO interactions with HBLC becomes stronger. This confinement is increasing because thermal energy and the rotational mobility of the nanowires were expanded. Precisely, a detailed investigation reveals that the customary crossover complex ZnO/HBLC nanocomposite module was sandwiched between the cells and temperature dependent textural phase distribution matrix appeared due to the introduction of nanowires into the host HBLC compound. It was noticed that the shiny nanofabric sheets of 'marble' patterns are appeared at temperature 112.5°C. The Fig. 2c signifies 'ON' (≥ 5 V) and 'OFF' (≤ 0 V) state electro-optical switching at the tilt angle ($\theta/4$) of contact. Thus, we may predict that POM can be revealed in various phases in different textural phase appearance, rotational mobility and, consequently, electro-optical (EO) switching ("ON"/"OFF") state is the main evidence of the influence of smooth dispersion of nanomaterials with LC, as well as acting as a surface stabilizing electro-optical cell.

2.5 Materials Characterizations by Spectroscopic Investigations

In the field of '*Liquid Crystal Nanoscience (LCN)*' Prof. K. Pal's group and his co-workers [33, 34], has quickly evolved during last decades, primarily due to our experimental ability with the help of modern instruments. ZnO

nanomaterials encapsulated with liquid crystalline materials hybrid nanocomposite products were grown on SiO_2 substrates and characterized by Field Emission Scanning Electron Microscopy (FE-SEM; Model: SIGMA ZEISS FE-SEM) using a JEOL electron microscope 6700 associated with a field emission gun operating at 3 kV. The chemical elemental distribution was detected by the MERLIN compact energy dispersion spectroscopy (EDS) detector. The thin-film surface morphology and surface current were investigated via tapping and conducting mode atomic force microscopy (Model: TP-AFM/C-AFM Multimode8, Bruker). The formation of 'H-'bond in liquid crystal was confirmed by NICOLET 5700 FTIR Spectrometer (Model: Continue μm IR Microscope), mid-infrared 4000–400 cm^{-1}, resolution 4 cm^{-1}, high resolution of 0.09 cm^{-1}. The HBLC complexes are analyzed using Nuclear magnetic resonance spectroscopy (NMR; Model: Brucker international model ULTRA SHIELD of 300 MHz). Smectic uniform lying helical texture patterns of electro-optical switching at various temperature were investigated by polarizing optical microscopy (Model: OLYMPUS, CX31, 6J09934 Japan) with a signal generator U8031A. Differential scanning calorimetric (DSC; Shimadzu DSC-60) helps to take the transition temperatures and corresponding enthalpy values. Semiconductor characterization system (Model: 4200-SCS) analyzes capacitance versus voltage (C-V) hysteresis loop and DC bi-stable switching of I-V response characteristics of controllable frequency 10 kHz. Correspondingly a digital source meter (Model: Agilent 33522A) of 30 MHz function generator utilized for an arbitrary waveform.

3 Results and Discussion

3.1 Spectroscopic Structure Analysis

3.1.1 Field-Emission Scanning Electron Microscopy (FE-SEM)

Primarily, we prepared hydrogen-bonded LC compounds (e.g. azelaic acid combined with p-n-pentyloxy benzoic acids (AC + 5BAO) and azelaic acid combined with p-n-heptyloxy benzoic acids (AC + 7BAO) and ZnO NWs. Typical growth dynamics were observed using FE-SEM on a large (several square centimetres) silicon wafer coated with nickel. The ratio of hydrogen to methane in the gas mixture and the reaction time were optimized in order to obtain a homogeneous and continuous layer with high coverage of the substrate surface. The FE-SEM images in Fig. 3 illustrate that hydrogen gas is vital for the growth of the nanomaterials. The semiconductor ZnO NW's is unidirectionally incorporated into the LC

solution, and two different types of worm-like morphology are seen (Fig. 3a–b). ZnO nanowires (of diameter ~ 30 nm) were used as a dopant in dilute liquid crystal solution, as depicted in Fig. 3c. However, those nanowires were gradually encapsulated by the liquid crystalline layer, and a hybrid NDLC compound matrix was formed, as depicted in Fig. 3d. The FE-SEM images clearly show promise for further significant attempts at the design and modulation of transparent electronic devices. A range of experiments were then performed to explore the unique properties of nanowire LC composites that could potentially be harnessed in novel switchable devices.

3.2 High-Resolution Transmission Electron Microscopy (HR-TEM), Energy Dispersion Spectroscopy (EDS) and Chemical Mapping

Typically, for HR-TEM imaging, ZnO/HBLC hybrid composite materials were transferred onto a copper-coated TEM grid followed by selective dissolution in ethanol. The HR-TEM sample was sliced to a thickness of 10 nm perpendicular to the carbon-coated copper grid at an acceleration voltage of 200 kV. Atomically resolved HR-TEM images (Fig. 4a) were used to characterize the atomic structure.

The ZnO NWs were completely capped by the liquid crystal layer, as they formed nanoparticle hybrid structures that exhibit overall surface uniformity. The HR-TEM images show that nanowires with diameters ranging from ~ 10 nm to several tens of nm were aggregated on the homogeneous surface. In some places along the HBLC-layer boundaries, a crystal face of the LC layer can be distinguished from the angles of the edges. However, close study of the HR-TEM images of the ZnO/HBLC hybrid composite shows bends and edges of the ZnO nanowires homogeneously dispersed in the LC in several places.

Next, we carried out EDS in order to observe well-anchored structure containing ZnO NWs of average diameter (~ 10 nm) that was homogeneously dispersed within the liquid crystalline surface. The ZnO/HBLC nanocomposite was randomly distributed on the layer, and the presence of the ZnO was helpful in preventing the HBLC from aggregation. The EDS patterns are shown in Fig. 4b confirm the atomic ratios of zinc (Zn-28.95%) and oxygen (O-20.35%). The Zn-atom concentration of the reduced ZnO/LC nanocomposite increased due to the loss of a portion of the oxygen-containing functional groups.

The elemental distribution was investigated by chemical mapping. We investigated the oxygen (O) content of the
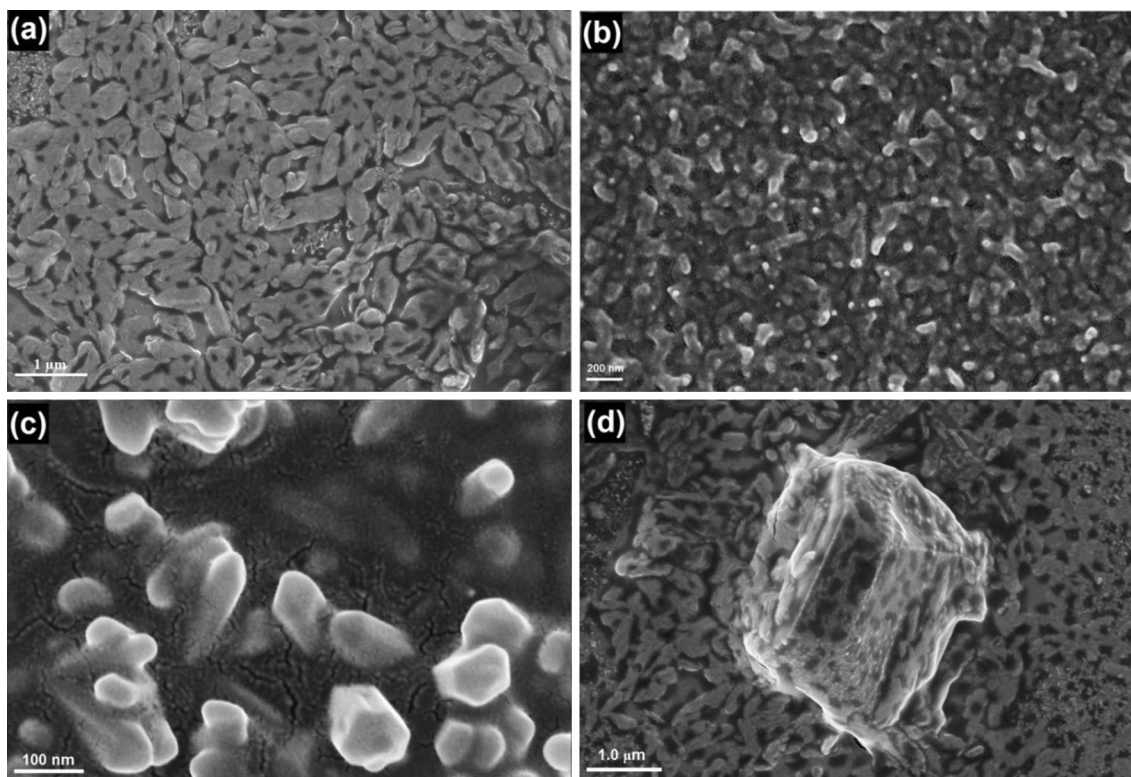

Fig. 3 FE-SEM micrographs of **a** HBLC: azelaic acid combined with p-n-pentyloxy benzoic acids (AC+nBAO), n=5 series. Scale bar: 1.0 μm, **b** The worm-like morphology corresponding to azelaic acid combined with p-n-heptyloxy benzoic acids (AC+nBAO) in an n=7 series. Scale bar:200 nm, **c** top view of the homogeneous dispersion of ZnO NWs in the HBLC compound, **d** smooth dispersion of the nanowire dopant in the hybrid composite matrix during gradual encapsulation by the formation of the liquid crystal layer
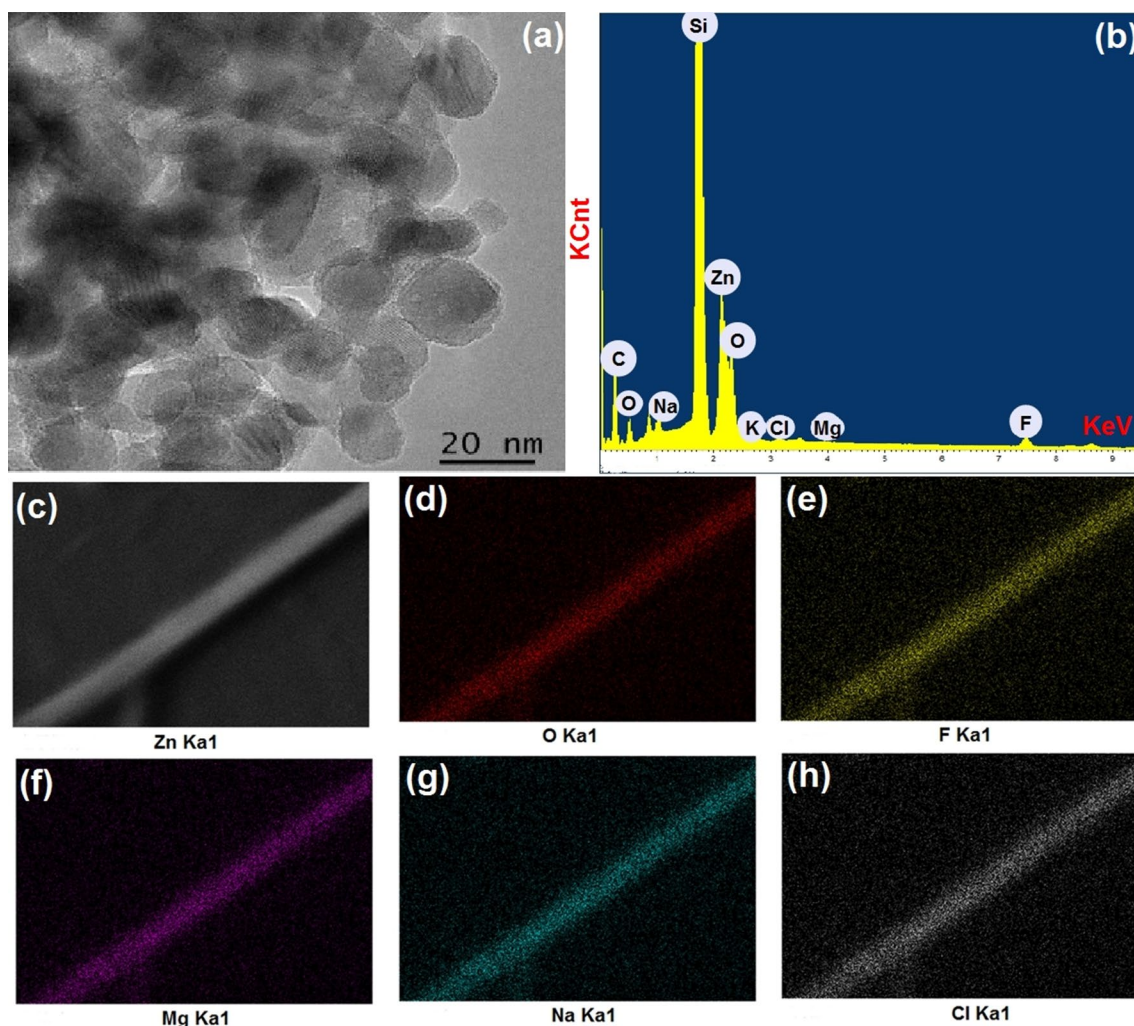
Fig. 4 **a** HR-TEM image of ZnO NWs dispersed in the HBLC hybrid nanocomposite material in an ethanol-based solution; **b** distribution of chemical elements in self-assembled ZnO nanowire/liquid crystal composite spin-coated on a silicon wafer substrate, as determined by EDS, **c–h** percentage (%) elemental distribution obtained through chemical mapping: zinc (Zn),oxygen (O), fluorine (F), magnesium (Mg), sodium (Na), and chlorine (Cl),corresponding to K_α orbital shells of the LC compounds

reduced HBLC is only 65.5%, and the mass percentage of Zn is 6.9% (Fig. 4c-h). The results also indicate that some O-containing functional groups were still present. The presence in the host HBLC compound of the elements fluorine (F), magnesium (Mg), sodium (Na), and chlorine (Cl), corresponding to 'Kα1' orbital shells was also confirmed.

3.3 Tapping/Conductive-Probe Atomic Force Microscopy (TP-AFM/C-AFM)

Next, we measured the local surface properties of the nanowires incorporated HBLC hybrid composites by using TP-AFM (surface topology investigation) and C-AFM (for surface current investigation), as depicted in Fig. 5a–b. The calculated surface roughness was on the order of 185 nm, and the average thickness of the thin film was approximately 105.9 nm due to the hybrid nanocomposite matrix (Fig. 5a). The most reliable surface current topography results obtained from the C-AFM profiles are shown in Fig. 5b. We found that the nanoparticle surface was uniformly distributed onto a silicon (Si) wafer by spin coating, which yielded a completely homogeneous dispersion covered by a metal coating and thus excellent conduction through the surface area. Surface currents on the order of nA which were obtained by applying a small bias field to the sample-AFM determined that initial surface-current values ranged from 4.7 to 12.3 nA, reaching saturation within the DC sample at a bias of 2 V. The reverse-biased current flow reached − 10 V and then returned ('red' line) to a value comparable to that of the reference current ('blue' line).
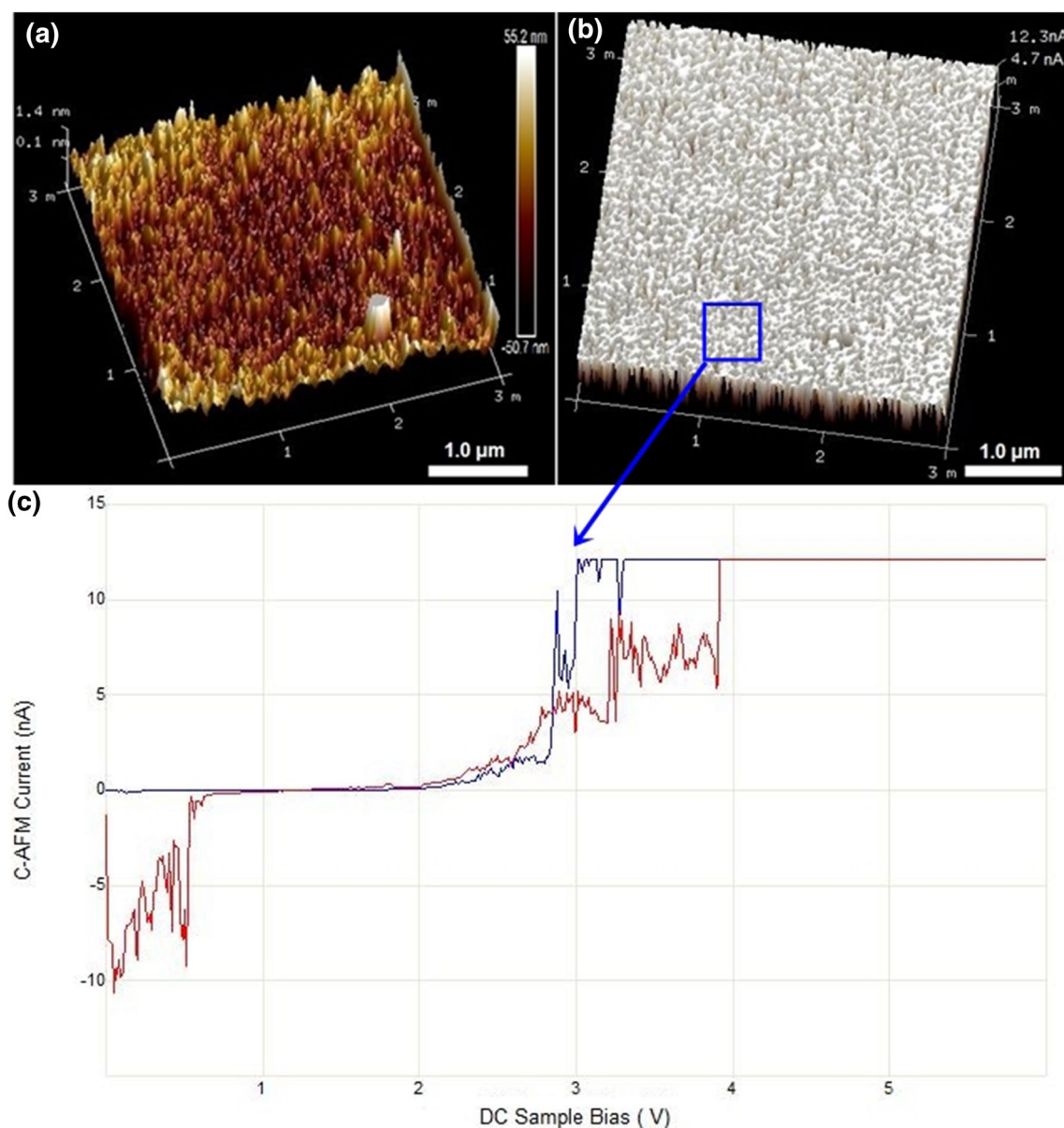
Fig. 5 Thin-film surface morphology investigation of ZnO nanowires encapsulated liquid crystals were prepared on a silicon wafer. **a** TP-AFM image used to determine the thickness, height and properties of the as-prepared metallic surface area. **b** maximum surface roughness of the as-prepared metallic surface area, **c** surface-current topology C-AFM as a function of externally-applied DC bias for the selected current through the conducting surface

3.4 FT-IR and NMR Investigation

The FT-IR spectrum of H-bonded liquid crystal compound (AC + nBAO; n = 5 and 7) is shown in Fig. 6a. The infrared spectra of free p-n-alkoxy benzoic acid, azelaic acid and their intermolecular H-bonded complexes were recorded in the solid state (Kerr) at room temperature. As a representative case, Fig. 6a illustrates the FT-IR spectrum of the hydrogen-bonded complex (AC + nBAO) series in the solid state at room temperature (31 °C). We observed two sharp bands, at 1685 and 1695 cm^{-1}, which can be interpret

as free alkoxy benzoic acid due to the ν(C=O) mode [35]. The doubling of this symmetrical stretching mode signal confirms the dimeric nature of alkoxy benzoic acid at room temperature [36]. The absorption peak at 3106 cm^{-1} is due to the C–H stretching of the aromatic systems, while the absorption at 1427 cm^{-1} is attributed to in-plane bending of O–H coupled with C–O stretching vibrations. In most samples of the HBLC (AC + nBAO) series, the O–H stretching absorption band appeared at 2924 cm^{-1}.

The presence of H-bonding in these complexes is further inferred from the appearance of a new band characteristic
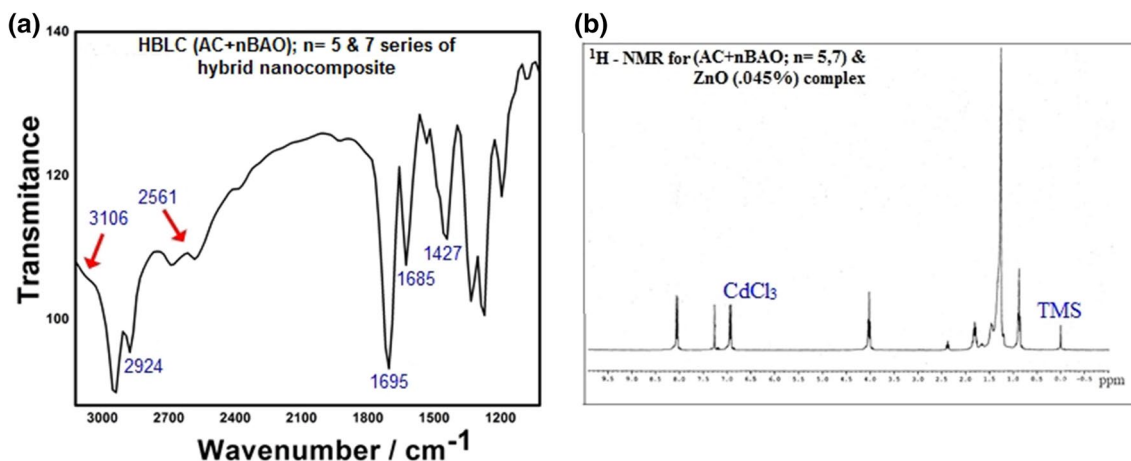
Fig. 6 FT-IR spectra of **a** H-bonded liquid crystal (AC + nBAO; n = 5 and 7) series compounds, and **b** ZnO NWs doped-HBLC hybrid composite matrix

of ν(O–H) at 2561 cm^{-1}. The doubling of the ν(C=O) mode signal may be attributed to the dimeric nature of the acid group at room temperature [33]. The corresponding spectrum of the solution state (chloroform) exhibits an intense and suggesting the existence of a monomeric form of benzoic acid. A noteworthy feature in the spectrum of the (AC + nBAO) series is the appearance of a broad band at 1690 cm^{-1} and the absence of the doubling of the ν(C=O) mode of the benzoic acid moiety. This characteristic clearly suggests that, the benzoic acid dimer dissociates and exists preferentially in a monomeric form upon complexation. As such, the FT-IR studies provide evidence of H-bond formation in both the above series. Moreover, the proposed structure of (AC + nBAO) complexes has been verified by ^{1}H-NMR studies.

As a representative case, we explored the ^{1}H-NMR of the (AC + nBAO) complex. The NMR spectrum of the complex is recorded in CdCl$_3$ with TMS as the internal standard. The recorded spectrum is shown in Fig. 6b, and the following chemical shifts were observed:

1. Broad resonance signals for methylene groups in the range of 0.5–2.8 ppm. In the (AC + nOBAO) complex, these signals were observed over the range 3.0–0.8 ppm and are attributed [37] to the existence of backbone methylene groups.
2. Two sets of multiples between 6.8–7.0 ppm and 8.0–8.1 ppm, equivalent to 2-H and attributed [38] to aromatic protons.
3. The methoxy proton unit resonance signal appeared between 3.9–4.0 ppm. The proposed structure of the complex was confirmed by the NMR study (Fig. 10b).

3.5 Dielectric Spectroscopy

Figures 7a, b show the frequency and temperature dependence of the dielectric constant 'ε'' and dielectric loss 'ε''' of a 0.045% ZnO nanowires doped HBLC hybrid composite. The response characteristics show that the dielectric constant decreases gradually as the frequency increases. This behaviour occurs due to the polarization of the synthesized sample lags behind the applied electric field.

The frequency dispersion dielectric data were recorded at frequencies ranging from 10 to 20 MHz by employing a low-frequency impedance analyzer. The thickness of the photo-refractive test cells were approximately 0.1 μm, thin enough to allow surface stabilization of the specimen. Frequency-dependent complex dielectric permittivity $\varepsilon^*(\omega)$ is determined by using the following equation [39, 40]:

$$\varepsilon * (\omega) = \frac{1}{j\omega C_0 Z^*(\omega)} = \frac{C_P}{C_0} - j\frac{1}{\omega C_0 R_P} = \varepsilon' - i\varepsilon'' \qquad (1)$$

where ε' is the dielectric constant, ε'' is the dielectric loss, 'j' denotes the square root of −1, ω (= 2Πf), is the angular frequency, 'Z' is the complex impedance, and C_0 and C_p are the capacitance of the cell under vacuum and filled with a dielectric bulk, respectively, R_p is the effective parallel resistance of the dielectric cell (consisting of a planar LC bulk in this study), and ε' and ε'' represent the real and imaginary parts of the complex dielectric constant, respectively.

The response characteristics further confirm that the dielectric constant of the ZnO/LC nanocomposite exhibited high values at low frequencies, which can be explained by using Maxwell–Wagner polarization theory [41]. This
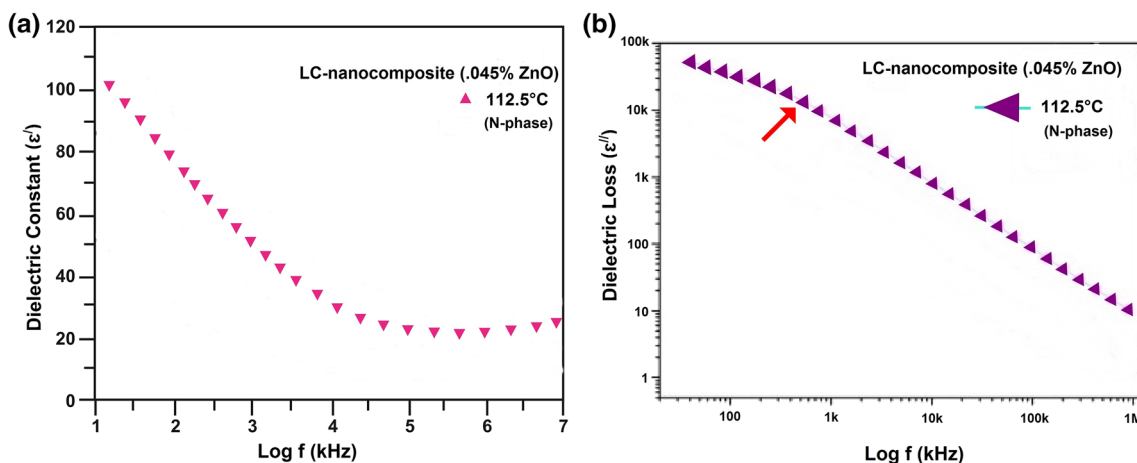
Fig. 7 Frequency variation dielectric dispersion characteristics of **a** dielectric-constant (ε') variation, and **b** dielectric-loss (ε'') variation in samples of ZnO nanowires doped into HBLCs (AC+nBAO) at a controllable fixed temperature of 112.5 °C, corresponding to the nematic (N) phase region (**Inset:** clearly distinguish relaxation peak by indicated 'Red' arrow). (Color figure online)

theory describes the heterogeneous structure of hybrid nanocomposites, in which a grain boundary separates the conducting grains and resistive grains. The grain-boundary volume dominates the dielectric constant at lower frequencies. When a nanomaterial is subjected to an electric field, free charge migration occurs, but the charges are trapped at the interfacial grain boundaries. This charge trapping leads to the formation of dipole moments at the boundaries, which in turn leads to space-charge polarization and ion-jump polarization. However, as the frequency increases, the dipoles cannot move sufficiently, resulting in deformation polarizability. Hence, they may not orient themselves along the direction of the applied electric field, which decreases the minimum dielectric permittivity.

The dielectric constants of ZnO nanowires which dispersed hybrid composites were observed to increase at a specific temperature [39, 40]. As the temperature increases, the number of thermally-activated charge carriers also increases. Hence, interfacial polarization develops due to the increased electron exchange interactions. The interfacial polarization is an important factor that increases the dielectric constant of the NDLC hybrid composite in the low-frequency region (corresponding to a temperature of 112.5 °C, the nematic phase), as shown in Fig. 7a. The dielectric-loss tangent (tan δ) describes the lag in the relaxation polarization that occurs due to the application of an electric field. The dielectric loss ε'' tangent of the ZnO nanowires as a function of frequency and temperature is shown in Fig. 7b. The dielectric loss decreases with increasing frequency. At frequencies below 1 kHz, the samples exhibit the highest dielectric loss ε'' values, whereas the value is completely independent of frequency in the higher-frequency region. This difference is

explained by the electron transfer and conductivity hopping of the material [41, 42]. In the lower-frequency region, electron transfer requires more energy. Thus the dielectric loss is manifested as a large hump (indicated by the red arrow) at frequencies higher than 1 kHz. In the highest-frequency region, which corresponds to low resistivity, electron transfer between the layers requires less energy. Furthermore, dielectric loss also increases with increasing temperature as a result of thermally-activated electron transfer. The incorporation of the NDLC sample also affected the dielectric loss [43, 44]. From details investigation through electrical measurements were influenced by two mechanisms, polarization due to the charge carrier displacement in the low frequency region and the contribution from the lattice at high frequencies.

3.6 AC Conductivity and Current Density

The frequency variation of the AC conductivity response, the temperature variation curve and the plot of current density against the bias voltage for the ZnO nanowires dispersed LC hybrid nanocomposite are illustrated in the Fig. 8a, b. The AC conductivity of the hybrid nanocomposite can be determined using the following equation [45–47]:

$$\sigma_{ac} = 2\pi\varepsilon_0\varepsilon_r f \tan\delta \qquad (2)$$

where ε_0 is the permittivity of free space, ε_r is the dielectric constant, f is the frequency, and tan δ is the loss factor. Figure 8a shows that in the low-frequency region, the electrical conductivity of the NDLC sample increases slowly with increasing frequency, and it is clear that the electrical conductivity also increases as the frequency increases. At the
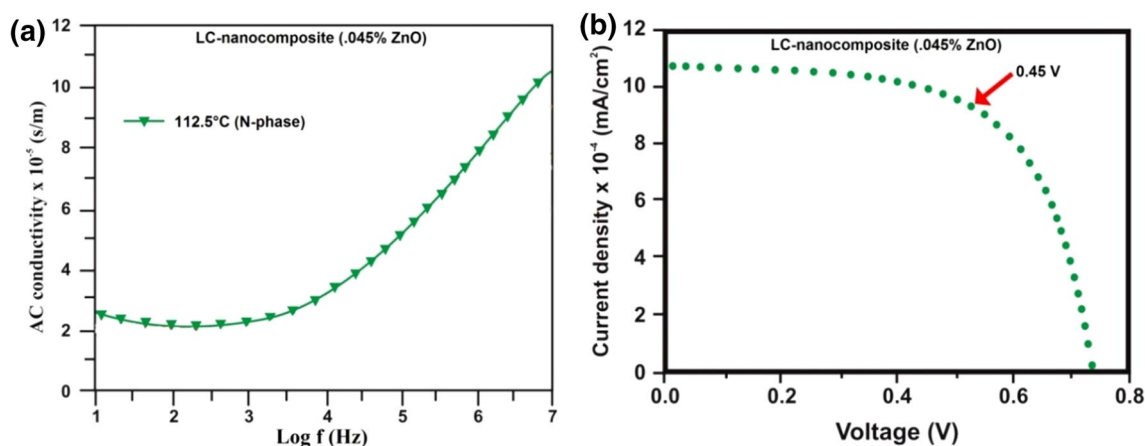
Fig. 8 **a** Frequency dependence of AC conductivity measured in the nematic phase at a fixed temperature of 112.5 °C, **b** current density as a function of voltage response for the ZnO NWs/LC hybrid nanocomposite

highest controllable temperature of 112.5 °C, in the nematic phase, a higher AC conductivity value was observed. It may predict frequency-independent behaviour at the lower-frequency region, which characterizes the DC conductivity, while the higher-frequency region exhibits frequency-dependent behaviour, which occurs due to the short-range translational hopping of charge carriers between the localized states. In the higher-frequency range, the AC conductivity of the material increases as the hopping frequency of the electrons is accelerated. As the temperature increases, the grain size also increases, but it is limited by the grain boundaries. However, the AC conductivity at high frequency is the tendency needed for small polaron hopping.

In the host nanomaterial, the conductivity relies on fairly localized carriers that are bound to the lattice with lattice strain due to polaron conduction [48]. The J-V characteristic curve of the ZnO/LC nanocomposite's photovoltaic performance is better, as can be seen in Fig. 8b. In the NDLC homogeneous composite system, ZnO is a better electron donor, while LC is a relatively good electron acceptor material, so the interaction between the two materials offers good electron transport. The conduction band of ZnO receives electrons from the HOMO level of the dye molecule. As the ZnO NWs remain anchored to the liquid crystal compounds, the excited electrons are easily captured. These electrons are then efficiently transported from ZnO to the conductive substrate via liquid crystal bridges, thus suppressing recombination. The AC conductivity behaviour is due to the hopping of oxygen vacancies.

3.7 Electrically-Influenced Switchable Supercapacitor Response

We usually determine that the interface quality capacitance–voltage (C-V) measurement can be an excellent option

as shown in Fig. 9a, b. The capacitance versus voltage (C-V) hysteresis curves of pure HBLC and ZnO nanowires-doped LC composites at a frequency of 10 kHz for an applied external bias voltage ranging from − 10 V to + 10 V. The Preisach model [49–51] was employed to fit the C-V curves. According to this model:

$$C = C_f + \sum_{i=1}^{n} \frac{P_{Si}.\delta_i.A}{\text{Cosh}^2\left[\delta_i.\left(V \pm V_{Ci}^{\pm}\right)\right]} \quad (3)$$

where C is the cell capacitance, C_f is the voltage-independent part of the capacitance, P_{si} is the spontaneous polarization of all dipoles in the i-th species fully aligned to an external field, A is the area of the cell, V_{Ci} is the coercive voltage at which the electrical polarization of the i-th species vanishes during switching from one orientation to the other, $\delta_i = V_{Ci}^{-1} \log\left\{\left[1 + \left(P_r/P_s\right)_i\right]/\left[1 - \left(P_r/P_s\right)_i\right]\right\}$ is the species-related constant, and P_r is the remnant polarization. We have neglected the contribution of the capacitance value from the alignment layer since it is very small. Critical analysis suggests exploration of the spontaneous polarization of all the 'two' and 'four' dipolar species from the fitted curves due to the pure HBLC (AC + nBAO; n = 5 and 7) series shown in Fig. 9a and the ZnO NWs doped LC-hybrid composite, as depicted in Fig. 9b.

We found that the peak capacitances decrease slightly in the doped cell. The bias voltage at which peak capacitance occurs is farther from 0 V in the doped cell than in the pure HBLC sample series. Detailed investigation suggests that the inherent dipole moment of the ZnO NWs enables them to interact antiparallel to the surrounding dipolar species in order to reduce the overall spontaneous polarization of the hybrid composite system.
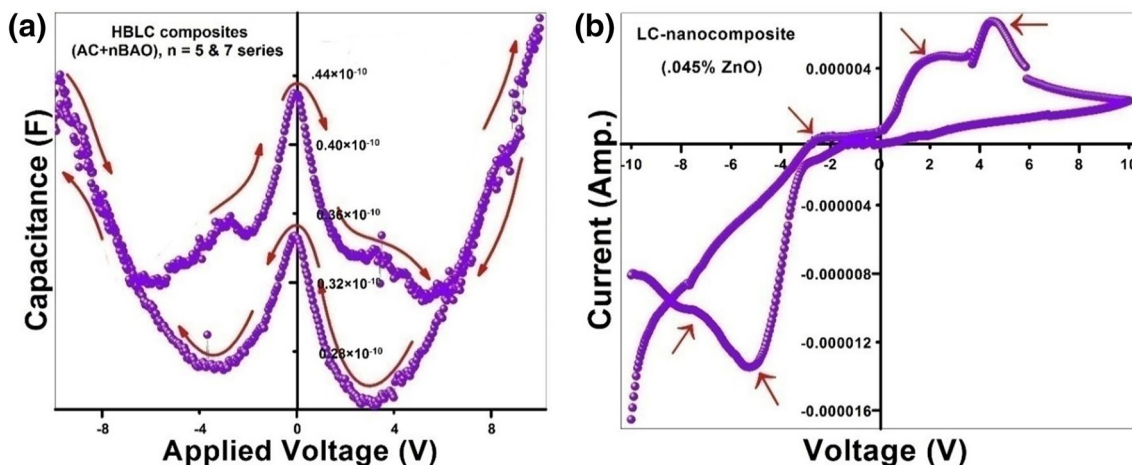
Fig. 9 Capacitance versus voltage hysteresis response at a fixed frequency of 10 kHz corresponding to **a** undoped ITO cells of the H-bonded liquid crystal (AC + nBAO; n = 5 and 7) compound series, and **b** doped ITO cells of the ZnO nanowires/LC hybrid nanocomposite material

3.8 Differential Scanning Calorimetry (DSC) Thermograms

Hence, the DSC thermograms were obtained during heating and cooling cycles (Fig. 10a, b). The ZnO NWs dispersed HBLC hybrid composite sample was heated with a scan rate of 10°C/min in a nitrogen (N₂) atmosphere and held at its isotropic temperature for 1 min to attain thermal stability. The cooling run was performed with the same scan rate of 10°C/min. The respective equilibrium transition temperatures and corresponding enthalpy values of the mesogens of the homologous series were recorded.

The typical phase-transition temperatures and corresponding enthalpy values of ZnO/HBLC hybrid compounds were investigated through the use of DSC thermograms, as

shown in Fig. 10a. The hydrogen-bonded complex thermogram was recorded at a scan rate of 10°C/min for the heating and cooling run. The cooling run of the DSC thermogram reveals four distinct transitions: isotropic (Iso) → nematic (N), nematic(N) → smectic C (Sm C), smectic C (Sm C) → smectic F (Sm F) and smectic F (Sm F) → crystal (Cr), with transition temperatures at 99.5 °C, 76.8 °C, 74.5 °C, 51.2 °C and corresponding enthalpy values of 0.75 J/g, 0.48 J/g, 5.93 J/g and 70.9 J/g, respectively. The heating cycle shows two distinct transitions, namely, from crystal to melt and from melt to nematic phases at 60.5 °C and 82.3 °C with corresponding enthalpy values of 75.27 J/g and 7.08 J/g, respectively. These transition temperatures are in agreement with optical polarizing microscopy studies [52, 53]. The sum of the enthalpies in the heating run
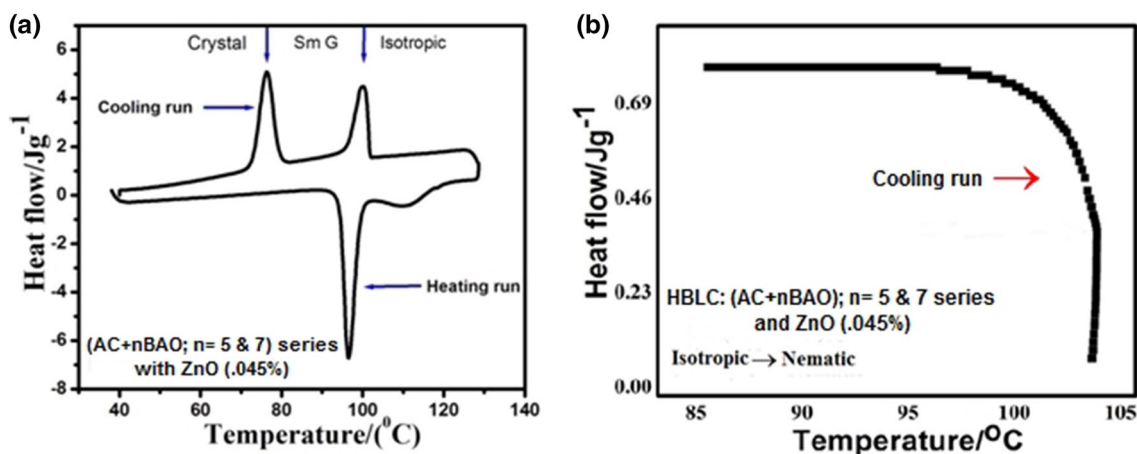

Fig. 10 Investigation of ZnO NWs homogeneously dispersed in hydrogen-bonded liquid crystalline materials (AC + nBAO; n = 5 and 7). **a** A typical DSC thermogram showing heating and cooling curves

reveals different phase variations, **b** 'Isotropic' to 'Nematic' phase transition during cooling run at high magnification

was 82.55 J/g, while that in the cooling run was 78.05 J/g, demonstrating that the mesogen effectively follows thermodynamic principles. Indeed, the enlarged DSC thermogram of the 'Iso→N' phase transition shown in Fig. 10b implies an excellent transition, which is classified as second order based on the enthalpy value. The phase transitions are classified as first and second order. The order of the transition can be evaluated by the magnitude of the enthalpy value. Further polarizing optical microscopy studies are also suggested by these DSC outcomes and the results of monotropic transition.

3.9 Study of Electro-Optical (EO)Properties

The EO properties of the hybrid nanocomposite device were characterized using a polarizing optical microscope (POM) positioned in the rubbing unidirection, oriented at 45° and crossing towards the polarizer. The thermotropic hydrogen-bonded liquid crystal which results directly from the combination of azelaic acid (AC) with p-n pentyloxy and p-n heptyloxy benzoic acids of carbon numbers 5 and 7 in a BAO homologous series causes birefringence, as observed under the polarizer, and when the dispersion is smooth. Figure 11 shows micrographs of aqueous HBLC compound solutions viewed through the polarizer. The typical shiny droplet pattern of the nematic (N) phase appeared at 126 °C (Plate 1), the conic texture of broken-foil smectic C (Plate 2) at 95 °C, and the threaded nematic schlieren texture (Plate 3) at 90.5 °C. The large schlieren texture area signifies regular orientation of the pure HBLC compound and, ultimately, transitions to the crystalline (Cr) phase at 85.5 °C. Moreover, the development of birefringence domains confirms the (Iso↔Cr) phase transition of the HBLC compound series. The different textural patterns of phase transitions were identified as follows:

(Isotropic 130 ↔ N 126 ↔ Sm C 95 → Cr 85.5)

The stable birefringence shows that smooth dispersions were obtained, and POM images reveal that the mesogens of ZnO NWs encapsulated HBLC hybrid composites exhibit phase transitions in different temperature regions and while cooling gradually at the isotropic temperature of 128.5 °C. Hence, the various textural patterns in Fig. 12:the shiny porous droplet product of the nematic (N) phase is observed at 126 °C (Plate1), while nematic (N) droplets with a porous pattern were obtained at 112.5 °C (Plate 2), and the 'multicolor parachromatic marble stripe' pattern of the smectic C* phase was obtained at 90.5 °C (Plate3). The smooth and shiny multi-coloured mosaic-type pattern of the smectic G* phase developed at 88.2 °C (Plate 4); at 81.5 °C the sample eventually entered a crystalline (Cr) phase. We thus observed new smectic ordering labelled Sm G*, which is sandwiched between the traditional nematic (N) and convectional Sm C* phases. The diagrammatic representation of peculiar textural phase (Iso↔Cr) patterns is obtained from the crystal-structure phase transitions of thisZnO/HBLC hybrid compound (AC+nBAO; n=5 and 7) series as follows:

(Isotropic 128.5 ↔ N 112.5

   ↔ Sm C ∗ 90.5 ↔ Sm G ∗ 88.2 → Cr 81.5

3.10 Electro-optical textural phase patterns

For a conventional hybrid composite consisting of ZnO nanowires assembled with the HBLC in a module sandwiched between two ITO cells, the temperature variation of the textural phase distribution matrix against carbon numbers (n=5 and 7) appeared as a result of the introduction of liquid crystalline compounds into the host structure, confirmed in Fig. 13. We may predict the essential points on the basis of experimental investigations as follows:
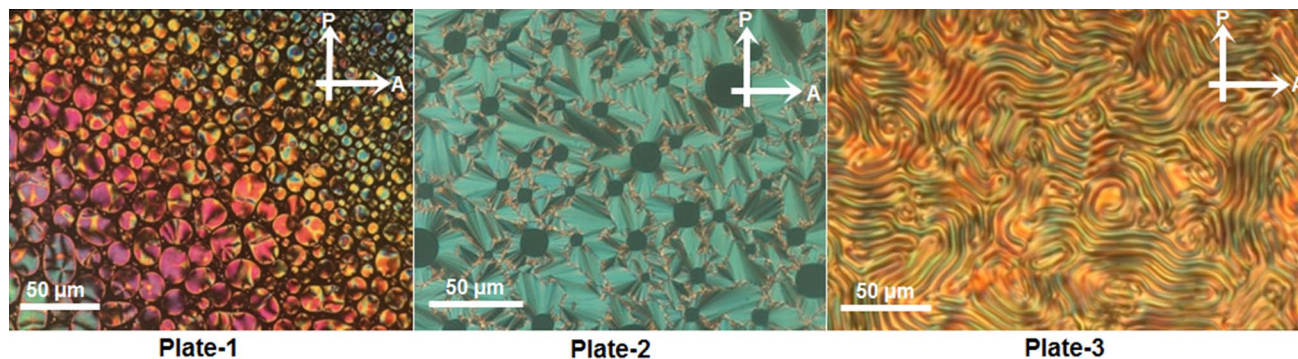

Fig. 11 Textures of optical micrographs were obtained under a cross polarizer with 20×magnification corresponding to a series of pure H-bonded liquid crystal compounds (AC+nBAO; n=5 and 7).The shiny droplet pattern of the nematic (N) phase appeared at 126 °C (Plate 1), the conic texture of broken foil smectic C (Plate 2) at 95 °C, and the threaded nematic schlieren texture (Plate 3) at 90.5 °C
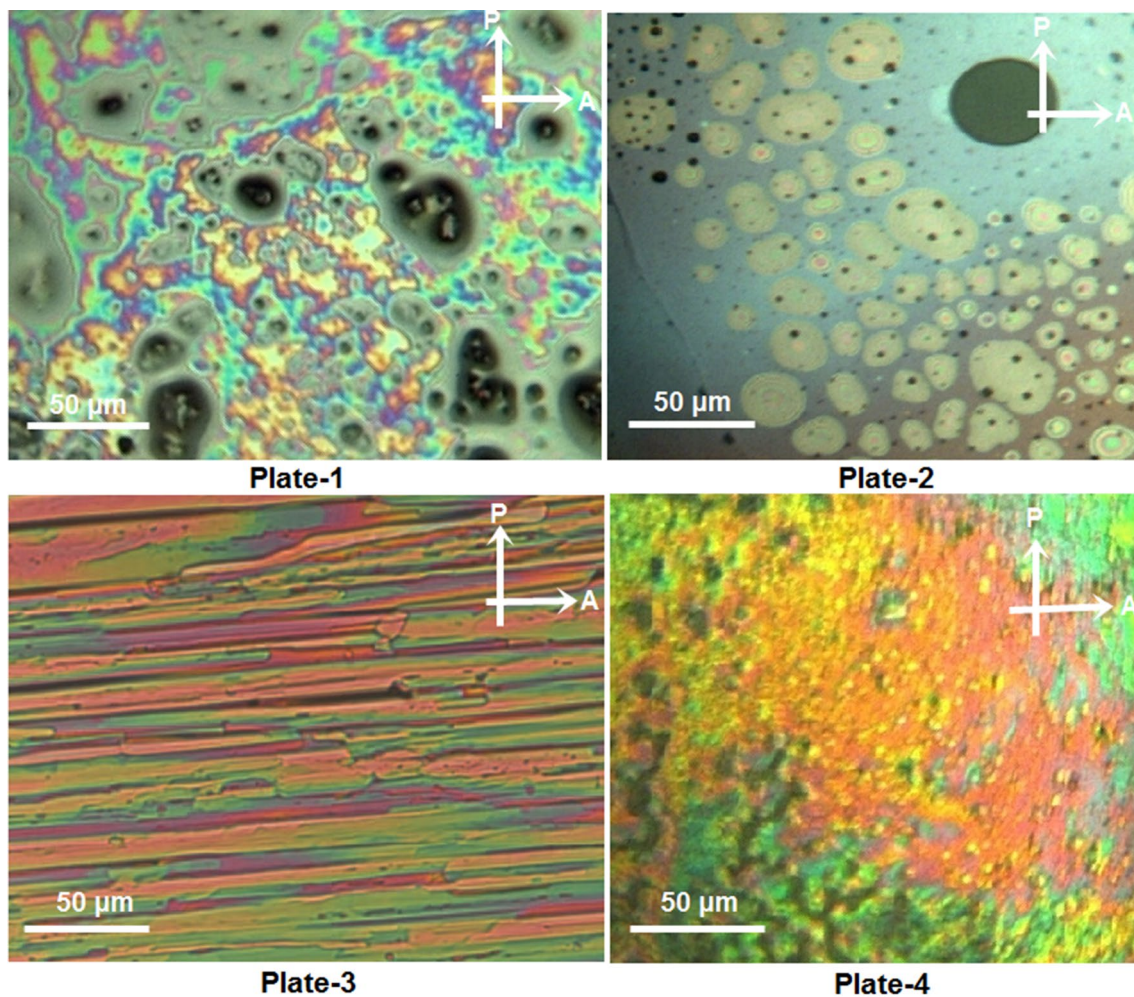
Fig. 12 A collection of optical micrographs showing the different textures under a cross polarizer at 10× magnification corresponding to ZnO nanowires homogeneously dispersed in an HBLC (AC + nBAO; n = 5 and 7) compound series. Shiny porous droplets in the nematic (N) phase pattern at 126 °C (Plate 1), traditional nematic (N) droplets with a porous pattern at 112.5 °C (Plate 2), smectic C* phase showing a multicolour parachromatic marble stripe patterns were obtained at 90.5 °C (Plate 3), and the smooth and shiny multi-coloured mosaic-like pattern of the conventional smectic G* phase developed at 88.2 °C (Plate 4)

(a) The phase diagram is composed of three phases e.g. Nematic, Smectic C*, and Smectic G*

(b) The nematic phase is present in all of the homologous series of the NWs dispersed HBLCs

(c) In the entire homologous series, in all complexes, the thermal range of the nematic phase is larger than that of the smectic G* phase

4 Conclusions

In this work, we demonstrate the creation of a LC-based hybrid composite matrix that incorporates a homogeneous dispersion of one-dimensional ZnO nanowires of 10 nm diameter to form a colloidal suspension. Using a range of spectroscopic tests, the influence of the ZnO NW's dopant concentration on the HBLC and its EO, dielectric spectroscopy behaviour of the matrix was explored. The nanowires open a route to controlling the EO properties of the LC system, and thus potentially point to novel switching mechanisms in LC and optoelectronics devices. The novel superior switching behaviour details illustrated here, could be harnessed in electro-optical investigations. The H-bonded mesogenic LCs at the heart of this work offer unique advantages. They can be tuned easily, simply by changing the H-bond donor and acceptor or the percentage of molar composition in order to obtain a complete dispersion. Indeed, their specific chemical structure can lead and give rise to new smectic ordering (Sm C*), which is sandwiched between the traditional nematic (N) and convectional Sm G* phases. Moreover, the temperature (112.5°C) at which the nematic phase is observed is close to the isotropic temperature, which could
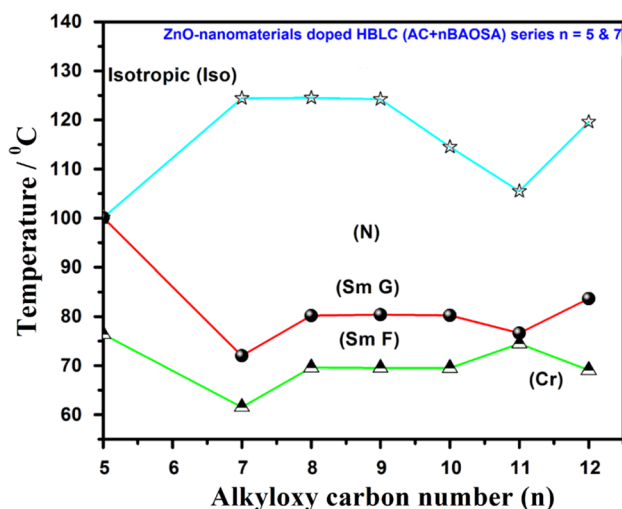
Fig. 13 Temperature-dependent phase variance of ZnO nanomaterial doped into homologous HBLC compound series with alkyloxy carbon numbers n = 5 and 7

prove beneficial for functionalizations. Overall, it is clear that the changes in LC orientation induced by the dispersion of nanomaterials will modify the transition temperature as well as induce textural phase changes. Both of these effects could prove useful in smart display applications at specific temperatures. Structural growth dynamical properties play a significant role in many areas, including chemical, physical and smart display technology. Thus, we may predict that while semiconductor nanomaterials have enjoyed a golden opportunity in novel trends in dynamic utilization in *"Liquid Crystal Nanoscience"*. So far, greater scope may be available to other nanomaterials also which can only be realized as the field moves forward and makes further advances in Nanotechnology.

Compliance with ethical standards

References

1. Kato, T., Mizoshita, N., Kishimoto, K.: Functional liquid-crystalline assemblies: self-organized soft materials. Angew. Chem. Int. Ed. **45**(1), 38–68 (2006)
2. Goodby, J.W., et al.: Transmission and amplification of information and properties in nanostructured liquid crystals. Angew. Chem. Int. Ed. **47**(15), 2754–2787 (2008)
3. Tschierske, C.: Liquid crystal engineering–new complex mesophase structures and their relations to polymer morphologies, nanoscale patterning and crystal engineering. Chem. Soc. Rev. **36**(12), 1930–1970 (2007)
4. Newsome, C., et al.: Laser etched gratings on polymer layers for alignment of liquid crystals. Appl. Phys. Lett. **72**(17), 2078–2080 (1998)
5. Kagajyo, T., et al.: Alignment of nematic liquid crystal molecules using nanometer-sized ultrafine patterns by electron beam exposure method. Jpn. J. Appl. Phys. **44**(1S), 578 (2005)
6. Varghese, S., et al.: Microrubbing technique to produce high pretilt multidomain liquid crystal alignment. Appl. Phys. Lett. **85**(2), 230–232 (2004)
7. Rüetschi, M., et al.: Creation of liquid crystal waveguides with scanning force microscopy. Science **265**(5171), 512–514 (1994)
8. Suh, D., Choi, S.J., Lee, H.H.: Rigiflex lithography for nanostructure transfer. Adv. Mater. **17**(12), 1554–1560 (2005)
9. Kim, S.R., et al.: Fabrication of polymeric substrates with well-defined nanometer-scale topography and tailored surface chemistry. Adv. Mater. **14**(20), 1468–1472 (2002)
10. Park, H.-G., et al.: Homeotropic alignment of liquid crystals on a nano-patterned polyimide surface using nanoimprint lithography. Soft Matter **7**(12), 5610–5614 (2011)
11. Bouteiller, L., Barny, P.L.: Polymer-dispersed liquid crystals: preparation, operation and application. Liq. Cryst. **21**(2), 157–174 (1996)
12. Spruce, G., Pringle, R.: Polymer dispersed liquid crystal (PDLC) films. Electron. Commun. Eng. J. **4**(2), 91–100 (1992)
13. Crawford, G.P., Zumer, S.: Liquid Crystals in Complex Geometries: Formed by Polymer and Porous Networks. CRC Press, Boca Raton (2014)
14. Armitage, D., Underwood, I., Wu, S.-T.: Introduction to Microdisplays, vol. 11. Wiley, Hoboken (2006)
15. Crawford, G.: Flexible Flat Panel Displays, p. 290. Wiley, Chichester (2005)
16. Hinojosa, A., Sharma, S.C.: Effects of gold nanoparticles on electro-optical properties of a polymer-dispersed liquid crystal. Appl. Phys. Lett. **97**(8), 081114 (2010)
17. Bozhevolnyi, S.I., Universitet, A., Shalaev, V.: Nanophotonics with surface plasmons-Part I. Photonics Spectra **40**(1), 58 (2006)
18. Shalaev, V.M.: Nanophotonics with Surface Plasmons—Part ll. Photonics Spectra (2006)
19. Barnes, W.L., Dereux, A., Ebbesen, T.W.: Surface plasmon subwavelength optics. Nature **424**(6950), 824 (2003)

20. Pal, K., et al.: Design, synthesis and application of hydrogen bonded smectic liquid crystal matrix encapsulated ZnO nano-spikes. J. Mater. Chem. C **3**(45), 11907–11917 (2015)

21. Pal, K., et al.: Influence of ZnO nanostructures in liquid crystal interfaces for bistable switching applications. Appl. Surf. Sci. **357**, 1499–1510 (2015)

22. Pal, K., et al.: Optical and electrical investigation of ZnO nano-wires array centre micro-flowers turn to hierarchical nano-rose structures. J. Nanosci. Nanotechnol. **15**, 1–10 (2016)

23. Pal, K., et al.: Synthetic strategy of porous ZnO and CdS nano-structures doped ferroelectric liquid crystal and its optical behav-ior. J. Mol. Struct. **1035**, 76–82 (2013)

24. Jiao, M., et al.: Alignment layer effects on thin liquid crystal cells. Appl. Phys. Lett. **92**(6), 061102 (2008)

25. Lu, S.-Y., Chien, L.-C.: Carbon nanotube doped liquid crystal OCB cells: physical and electro-optical properties. Opt. Express **16**(17), 12777–12785 (2008)

26. Toney, M.F., et al.: Near-surface alignment of polymers in rubbed films. Nature **374**(6524), 709 (1995)

27. Orbitals, I.F.F.: Organic Chemical Reactions. Wiley, New York (1976)

28. Ginzburg, V.: Some remarks on phase transitions of the second kind and the microscopic theory of ferroelectric materials. Soviet Phys. Solid State **2**, 1824–1834 (1961)

29. Berlyand, L.: Homogenization of the Ginzburg-Landau functional with a surface energy term. Asymptot. Anal. **21**(1), 37–59 (1999)

30. Bethuel, F., Brezis, H., Hélein, F.: Ginzburg-Landau Vortices, vol. 13. Springer, Berlin (1994)

31. Meyer, R.B., et al.: Equilibrium size and textures of islands in free-standing smectic C* films. Mol. Cryst. Liq. Cryst. Sci. Tech-nol. Sect. A Mol. Cryst. Liq. Cryst. **364**(1), 123–131 (2001)

32. Ericksen, J.L.: Liquid crystals with variable degree of orientation. Arch. Ration. Mech. Anal. **113**(2), 97–120 (1991)

33. Pal, K., et al.: Functionalized graphene oxide dispersed hydrogen bonded liquid crystals efficient electro-optical switching. J. Dis-play Technol. **12**(3), 281–287 (2016)

34. Pal, K., et al.: Efficient one-step novel synthesis of ZnO nano-spikes to nanoflakes doped OAFLCs (W-182) host: optical and dielectric response. Appl. Surf. Sci. **280**, 405–417 (2013)

35. Vijayakumar, V., Murugadass, K., Mohan, M.: Inter hydrogen bonded complexes of hexadecylaniline and alkoxy benzoic acids: a study of crystallization kinetics. Braz. J. Phys. **39**(3), 600–605 (2009)

36. Nakamoto, K., Nakamoto, K.: Infrared and Raman Spectra of Inorganic and Coordination Compounds. Wiley, Hoboken (1977)

37. Vijayakumar, V., Madhu Mohan, M.: Experimental evidence of an optical shutter in cholesteric phase of a double hydrogen bonded liquid crystal. Braz. J. Phys. **39**(4), 677–683 (2009)

38. Guthrie, R.D.: Introduction to Spectroscopy (Pavia, Donald; Lampman, Gary M.; Kriz, George S., Jr.). ACS Publications, Washington (1979)

39. AL-TURKI, A.M.: Effect of preparation methods on the particles size, dielectric constant and antibacterial properties of ZnO nano-particles and thin film of ZnO/Chitosan. Orient. J. CHEM. **34**(1), 548–554 (2018). https://doi.org/10.13005/ojc/340163

40. Hsu, S.C., et al.: Effect of the polyimide structure and ZnO con-centration on the morphology and characteristics of polyimide/ZnO nanohybrid films. Macromol. Chem. Phys. **206**(2), 291–298 (2005)

41. Wu, C., et al.: Morphology-controllable graphene–TiO 2 nanorod hybrid nanostructures for polymer composites with high dielectric performance. J. Mater. Chem. **21**(44), 17729–17736 (2011)

42. Ahmad, K., Pan, W., Wu, H.: High performance alumina based graphene nanocomposites with novel electrical and dielectric properties. RSC Adv. **5**(42), 33607–33614 (2015)

43. Jammula, R.K., et al.: Strong interfacial polarization in ZnO deco-rated reduced-graphene oxide synthesized by molecular level mix-ing. Phys. Chem. Chem. Phys. **17**(26), 17237–17245 (2015)

44. Wang, D., et al.: Functionalized graphene–BaTiO 3/ferroelectric polymer nanodielectric composites with high permittivity, low dielectric loss, and low percolation threshold. J. Mater. Chem. A **1**(20), 6162–6168 (2013)

45. Roy, A.K., et al.:, Electrical Properties and AC Conductivity of (Bi 0.5 Na 0.5) 0.94 Ba 0.06 TiO 3 Ceramic. ISRN Ceramics (2012)

46. Almond, D.P., Bowen, C.: Anomalous power law dispersions in ac conductivity and permittivity shown to be characteristics of microstructural electrical networks. Phys. Rev. Lett. **92**(15), 157601 (2004)

47. Bowen, C., Almond, D.P.: Modelling the'universal'dielectric response in heterogeneous materials using microstructural elec-trical networks. Mater. Sci. Technol. **22**(6), 719–724 (2006)

48. Raghasudha, M., Ravinder, D., Veerasomaiah, P.: Influence of Cr3 + Ion on the Dielectric Properties of Nano Crystalline Mg-Ferrites Synthesized by Citrate-Gel Method. Materials Sciences and Applications **04**(07), 7 (2013)

49. Miller, S., et al.: Device modeling of ferroelectric capacitors. J. Appl. Phys. **68**(12), 6463–6471 (1990)

50. Miller, S., et al.: Modeling ferroelectric capacitor switching with asymmetric nonperiodic input signals and arbitrary initial condi-tions. J. Appl. Phys. **70**(5), 2849–2860 (1991)

51. Yang, P., et al.: Electrical properties of SrBi 2 Ta 2 O 9 ferro-electric thin films at low temperature. Appl. Phys. Lett. **81**(24), 4583–4585 (2002)

52. Si, G., et al.: Liquid-crystal-enabled active plasmonics: a review. Materials **7**(2), 1296–1317 (2014)

53. Ma, R., et al.: Synthesis of CdS nanowire networks and their opti-cal and electrical properties. Nanotechnology **18**(20), 205605 (2007)